Valley-dependent properties in two-dimensional Cr$_2$COF MXene predicted from first principles

Xiangyu Feng, Zhonglin He, Rui Peng, Ying Dai,[*] Baibiao Huang, and Yandong Ma[†]

School of Physics, State Key Laboratory of Crystal Materials, Shandong University, Shandanan Street 27, Jinan 250100, China

The search for valley-dependent exotic properties could enable quantum device applications and therefore attracts rapidly increasing attention. Here, using first principles, we predict existence of the intrinsic valley-related multiple Hall effect in two-dimensional (2D) Cr$_2$COF MXene. Cr$_2$COF MXene is a ferromagnetic semiconductor with a direct bandgap locating at the edges of the hexagonal Brillouin zone, endowing it with valley physics. Protected by time-reversal symmetry breaking and out-of-plane magnetization, the valleys are polarized spontaneously. Moreover, the valley polarization is sizeable in both the valence and conduction bands, benefiting the observation of the anomalous valley Hall effect. More remarkably, due to strong spin-orbit interaction, the valley-dependent band inversion occurs naturally, and thus, the valley-polarized quantum anomalous Hall effect can be realized simultaneously in Cr$_2$COF MXene, giving rise to the intriguing intrinsic valley-related multiple Hall effect. In addition, this multiple Hall effect can be effectively engineered under strain. Our findings greatly enrich the research on valley-dependent physical properties in 2D systems.

I. INTRODUCTION

Valley, referring to the degenerate energy extrema in momentum space, is an emerging degree of freedom of carriers in analog to charge and spin [1]. There are many intrinsic physical properties associated with valley occupancy, such as the Berry curvature, orbital magnetic moment, and optical circular dichroism, which enables the ability to control valleys [2]. This electronic degree of freedom can give rise to unconventional valley-dependent physics and device applications [3–6]. For example, by distinguishing and manipulating carriers at the valleys, the valley polarization and thus valley Hall effect can be realized [5–7]. In this regard, the valley index can be utilized as an information carrier, leading to the concept of valleytronics [8]. Due to the large separation in momentum space, the valley index in two-dimensional (2D) lattice is robust against smooth deformation and low-energy phonons, making it promising for information processing and storage. The current research for achieving valley polarization has been mainly established in the paradigms of external approaches, which suffers from various problems [9–19]. To conquer these challenges, the exotic anomalous valley Hall (AVH) effect [20], rooted in spontaneous valley polarization in 2D ferromagnetic semiconductors, is recently proposed. For the valley Hall effect in ferromagnetic materials, it possesses a more interesting feature, that is, the presence of additional charge Hall current, which is referred to as AVH effect [20]. Nevertheless, the spontaneous valley polarization has been reported in only a few 2D systems so far [20–26]. Most of these few existing systems harbor the annoying in-plane magnetization [21,23,26].

The coupling between valley and topology physics can yield another intriguing valley-dependent phenomenon, namely, the valley-polarized quantum anomalous Hall (VP-QAH) effect [27,28]. Different from common QAH effect, the VP-QAH is represented by a gapless surface/edge state connecting the conduction band of one valley to the valence band of another valley rather than in a single valley [29,30]. The VP-QAH effect can be characterized by quantum Hall resistance and zero longitudinal resistance [31,32]. These characteristic features have a topological origin, which are protected from elastic backscattering, and therefore hold potential applications for low power quantum computation [33]. Compared with either AVH effect or VP-QAH effect, undoubtedly, their simultaneous existence (i.e., valley-related multiple Hall effect) in 2D systems is more striking. That is because the realization of valley-related multiple Hall effects can offer the unprecedented opportunity to achieve robust dissipationless valleytronics [28]. Though highly valuable, arising from the required band inversion at the valley, the appearance of the VP-QAH effect usually deforms the valley features; thus, it is accompanied with the vanishing of the AVH effect [28,34,35]. As a result, up to now, the valley-related multiple Hall effects, especially being intrinsic, have been rarely explored [29,30,36,37].

MXene, representing 2D transition metal carbides and nitrides, becomes one of the hopeful candidates for 2D materials following the synthesis of Ti$_3$C$_2$ [38,39]. The general formula of MXene can be written as $M_{n+1}X_nA$ (M is a transition metal; X represents C or N; A represents O, F, OH, or Cl; and $n = $ 1–3). Based on the intrinsic ferromagnetism (FM) of Cr$_2$C, surface engineering can be used to break the inversion symmetry and retain the time-reversal symmetry breaking. Here, we present the discovery of intrinsic valley-related multiple Hall effects in 2D Cr$_2$COF MXene based on first-principles calculations. We find that it is a ferromagnetic semiconductor

---

[*]daiy60@sdu.edu.cn
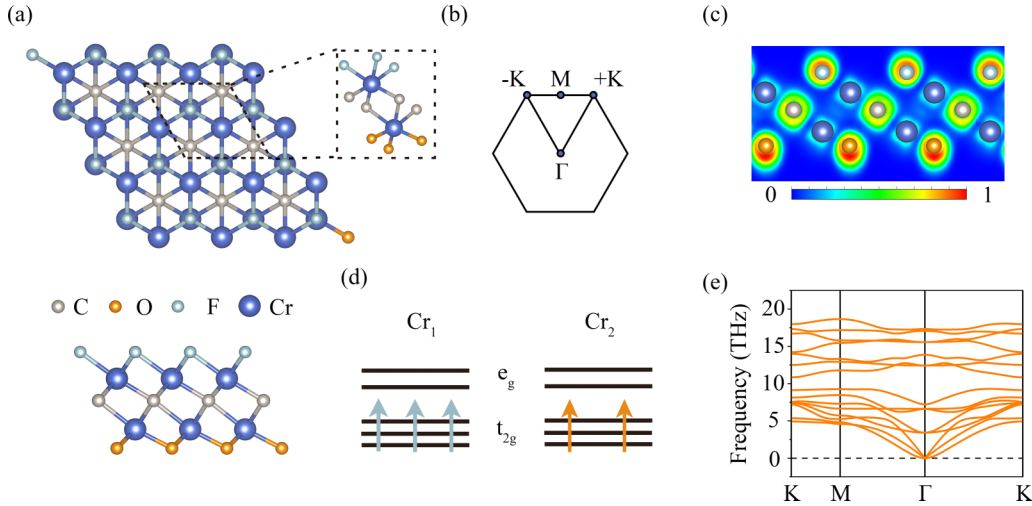
[†]yandong.ma@sdu.edu.cn

FIG. 1. (a) Crystal structure of Cr_2COF MXene from top and side views. (b) Two-dimensional (2D) Brillouin zone with marking the high-symmetry k points. (c) Electron localization function of Cr_2COF MXene. (d) Splitting of d orbitals of the Cr atom under the distorted octahedral crystal field. (e) Phonon spectra of Cr_2COF MXene.

with band edges locating at the $+K/-K$ points, giving rise to the valley physics. Importantly, the valleys are polarized spontaneously, which arises from the time-reversal symmetry breaking and out-of-plane magnetization, and the valley polarization is sizeable in both the valence and conduction bands. This benefits the observation of the AVH effect in Cr_2COF MXene. More intriguingly, the band order is inverted at the $+K$ valley, while it preserves as trivial at the $-K$ valley, presenting the VP-QAH effect. Such simultaneous existence of AVH and VP-QAH effects leads to the tantalizing intrinsic valley-related multiple Hall effects. Furthermore, we find that, under strain engineering, the characters of valley-related Hall effect can be modulated. These fundamental insights motivate a vista for seeking valley-related multiple Hall effects in 2D lattices.

II. METHOD

First-principles calculations are performed based on density functional theory as implemented in Vienna *Ab initio* Simulation Package [40–42]. The exchange-correlation interactions are treated by generalized gradient approximation in the form of the Perdew-Burke-Ernzerhof functional [43]. The cutoff energy is set to 500 eV. The vacuum space is set to 30 Å. The $11 \times 11 \times 1$ Monkhorst-Pack k-point mesh is used to sample the 2D Brillouin zone. All structures are fully relaxed until the atomic force on each atom is <0.01 eV/Å, and the convergence criterion of the total energy is set to 10^{-5} eV. Considering the strong correction effect for the localized $3d$ electrons of Cr atoms, we employ the Heyd-Scuseria-Ernzerhof hybrid functional [44] to calculate the band structures. Berry curvatures are calculated by employing the VASPBERRY package [45].

III. RESULTS AND DISCUSSION

Figure 1(a) displays the crystal structure of Cr_2COF MXene. It exhibits a hexagonal lattice with the space group of $P3m1$. Each unit cell contains one C, one O, one F, and two

Cr atoms, which are stacked in the sequence of F-Cr-C-Cr-O. Therefore, Cr_2COF MXene exhibits the intrinsic broken inversion symmetry. The lattice constant of Cr_2COF MXene is optimized to 2.968 Å, which is consistent with previous work [46]. To investigate the bonding characteristics of Cr_2COF MXene, we calculate its electron localization function in the plane containing F-Cr-C-Cr-O. As shown in Fig. 1(c), the electrons mainly localized around the atoms, while those in between the atoms are negligible, indicating an ionic bonding for all the bonds. The dynamically stability of Cr_2COF MXene is confirmed by the phonon spectra illustrated in Fig. 1(e), which exhibits the absence of imaginary frequencies in the whole Brillouin zone.

The valence electronic configuration of the Cr atom is $3d^5 4s^1$. For the upper Cr atom (Cr_1), it would denote three electrons to the six neighboring F and C atoms, giving rise to the electronic configuration of $3d^3 4s^0$. While for the lower Cr atom (Cr_2), due to the different coordinated atoms, one more electron would be transferred to the neighboring atoms, and the electronic configuration of Cr_2 would be $3d^2 4s^0$. For both Cr_1 and Cr_2 atoms, they are under a distorted octahedral coordination environment, and the d orbitals are roughly split into two groups [Fig. 1(d)]. As illustrated in Fig. 1(d), the three left electrons of the Cr_1 atom would half fill the t_{2g} orbitals, yielding a magnetic moment of 3 μ_B. For the Cr_2 atom, the two left electrons would half fill two of these three orbitals, leading to a magnetic moment of 2 μ_B. As expected, our spin-polarized calculations show that Cr_2COF MXene is spin polarized, and the magnetic moment per unit cell is calculated to be 5 μ_B, which is mainly distributed on the Cr atoms.

By examining the crystal structure of Cr_2COF MXene, we find that the Cr-C-Cr bonding angle is close to 90°. According to Goodenough-Kanamori-Anderson rules [47–49], FM coupling would dominate the magnetic coupling among the magnetic moments of Cr_2COF MXene. To firmly confirm the magnetic coupling of Cr_2COF MXene, we consider four magnetic configurations, i.e., FM and three types of antiferromagnetic ones (AFM1, AFM2, and AFM3; Fig. S1 in the
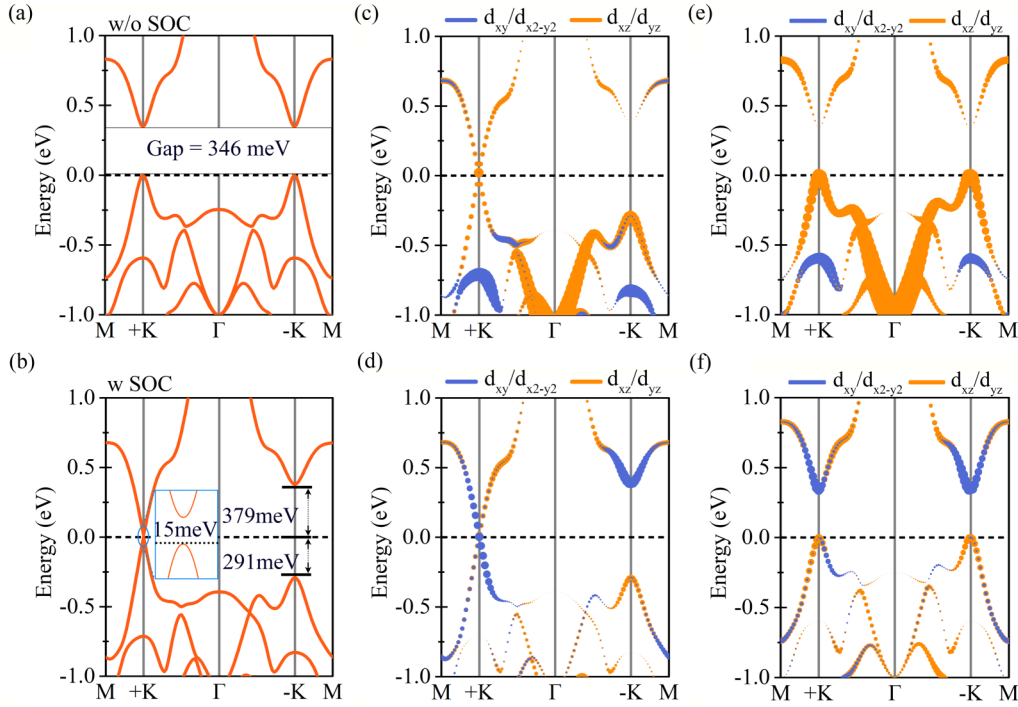
FIG. 2. Band structures of Cr_2COF MXene (a) without and (b) with considering spin-orbit coupling (SOC). Band structures of Cr_2COF MXene with considering SOC projected on the d orbitals of (c) Cr_1 and (d) Cr_2 atoms and without considering SOC projected on the d orbitals of (e) Cr_1 and (f) Cr_2 atoms. The Fermi level is set to the valence band maximum.

Supplemental Material [50]). Indeed, Cr_2COF MXene prefers FM coupling, which is 358, 737, and 622 meV lower in energy than the AFM1, AFM2, and AFM3 couplings, respectively. Furthermore, the magnetic anisotropy energy (MAE) of Cr_2COF MXene is calculated to determine its magnetization easy axis. The magnetization orientation of Cr_2COF MXene is found to be out-of-plane with a large MAE of 1 meV per unit cell, which is significantly larger than those of Ni, Fe, and Co [51] and comparable with those of CrI_3, MnB_6, and $MnGaX_3$ [52–55]. Such a sizeable MAE value indicates that the out-of-plane magnetization is robust, which benefits for establishing the long-range magnetic order [56] as well as the emergence of valley polarization discussed later.

Figure 2(a) presents the band structure of Cr_2COF MXene without considering spin-orbit coupling (SOC). Due to the large spin polarization, the bands around the Fermi level are only from the spin-up channel. It is a semiconductor with a direct bandgap of 346 meV. Therefore, Cr_2COF MXene is a 2D ferromagnetic semiconductor. Its valence band maximum (VBM) and conduction band minimum (CBM) both locate at the $+K/-K$ points, which are mainly contributed by $d_{xz/yz}$ orbitals of the Cr_1 atom and d_{xy/x^2-y^2} orbitals of Cr_2 atoms; see Figs. 2(e) and 2(f). Given the intrinsic broken inversion symmetry, the band edges form a pair of energetically degenerate valleys in both the conduction and valence bands of Cr_2COF MXene. When taking SOC into consideration, as shown in Fig. 2(b), the degeneracy between $+K$ and $-K$ valleys is lifted. In detail, the $+K$ valley shifts below the $-K$ valley in the conduction band, while the $+K$ valley shifts above the $-K$ valley in the valence band. Therefore, the valley polarization is realized spontaneously in both the conduction and valence bands of Cr_2COF MXene. The spontaneous

valley polarization of Cr_2COF MXene arises from the joint effect of magnetic exchange interaction and SOC. Importantly, the spontaneous valley polarization is sizeable for both the conduction and valence bands, which is 364 and 291 meV, respectively. Such values are comparable with those of NbX_2 and GdI_2 [24,26], which would facilitate the observation of the AVH effect. It is worthy emphasizing that the spontaneous valley polarization in Cr_2COF MXene is different from most of the previously studied 2D valleytronic systems [20–26], wherein such sizeable spontaneous valley polarization usually occurs in either the conduction or the valence band but not both.

We then explore the underlying physics for this discrepancy. From the orbital-resolved band structures of Cr_2COF MXene without considering SOC shown in Figs. 2(e) and 2(f), it can be seen that the CBM is dominated by $d_{x^2-y^2/xy}$ orbitals of the Cr_2 atom, and the VBM mainly comes from $d_{xz/yz}$ orbitals of the Cr_1 atom. Because SOC plays an important role in realizing the valley polarization, we employ a simple effective model to study the SOC effect. Considering the states around the Fermi level are from one spin channel, the Hamiltonian of SOC $\hat{H}_{SOC}$ can be expressed as [57,58]

$$\hat{H}_{SOC} = \lambda \hat{S}_{z'}\left(\hat{L}_z\cos\theta + \tfrac{1}{2}\hat{L}_+ e^{-i\phi}\sin\theta + \tfrac{1}{2}\hat{L}_- e^{+i\phi}\sin\theta\right).$$

Here, $\hat{L}$ and $\hat{S}$ are the orbital angular and spin angular operators, respectively. Also, θ and ϕ indicate the spin orientations, respectively. As Cr_2COF MXene exhibit intrinsic out-of-plane magnetization orientation, $\theta = 0$, and then $\hat{H}_{SOC}$ can be simplified as

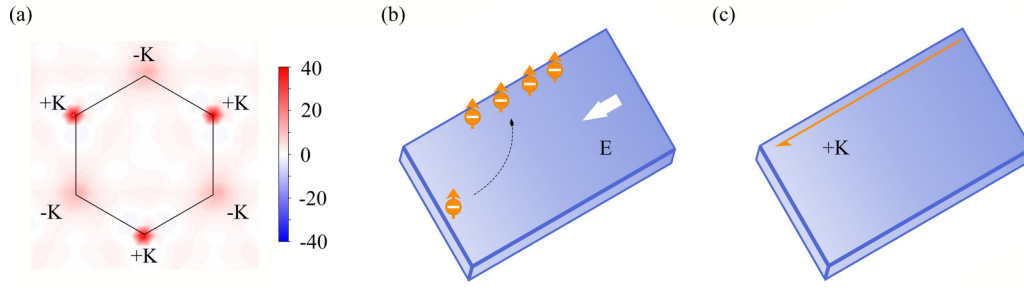$$\hat{H}_{SOC} = \lambda \hat{S}_{z'}\hat{L}_z.$$

FIG. 3. (a) Berry curvature of Cr_2COF MXene as a counter map over the two-dimensional (2D) Brillouin zone. (b) Diagram of the anomalous valley Hall (AVH) effect under electron doping. (c) Diagram of the valley-polarized quantum anomalous Hall (VP-QAH) effect under electron doping. The $-$ symbols represent electrons, and the orange upward arrows represent spin-up states.

Considering the orbital contribution around the valleys and the C_3 symmetry, the basis functions of conduction and valence bands can be chosen as

$$|\varphi_c^\tau\rangle = \sqrt{\frac{1}{2}}(|d_{x^2-y^2}\rangle + i\tau|d_{xy}\rangle),$$

$$|\varphi_v^\tau\rangle = \sqrt{\frac{1}{2}}(|d_{xz}\rangle + i\tau|d_{yz}\rangle).$$

Here, τ represents the valley index. Also, $c(v)$ indicates the conduction (valence) band. The energy levels of the $+K/-K$ valleys can be written as

$$E_c^\tau = \langle\varphi_c^\tau|\hat{H}_{SOC}|\varphi_c^\tau\rangle,$$

$$E_v^\tau = \langle\varphi_v^\tau|\hat{H}_{SOC}|\varphi_v^\tau\rangle.$$

As a result, the valley polarizations in both conduction and valence bands can be written as

$$E_c^{+K} - E_c^{-K} = i\langle d_{x^2-y^2}|\hat{H}_{SOC}|d_{xy}\rangle - i\langle d_{xy}|\hat{H}_{SOC}|d_{x^2-y^2}\rangle$$
$$= 4\alpha,$$

$$E_v^{+K} - E_v^{-K} = i\langle d_{xz}|\hat{H}_{SOC}|d_{yz}\rangle - i\langle d_{yz}|\hat{H}_{SOC}|d_{xz}\rangle = 2\beta.$$

Here, we have used $\hat{L}_z|d_{xz}\rangle = i|d_{yz}\rangle$, $\hat{L}_z|d_{yz}\rangle = -i|d_{xz}\rangle$, $\hat{L}_z|d_{x^2-y^2}\rangle = 2i|d_{xy}\rangle$, $\hat{L}_z|d_{xy}\rangle = -2i|d_{x^2-y^2}\rangle$, $\alpha = \lambda\langle d_{x^2-y^2}|\hat{S}_{z'}|d_{x^2-y^2}\rangle$, and $\beta = \lambda\langle d_{xz}|\hat{S}_{z'}|d_{xz}\rangle$. Due to the strong SOC in Cr-d orbits, α and β have large values. In most of the previous systems, due to the fact that the orbital composition d_{z^2} does not contribute to valley polarization, they only have valley polarization in either the conduction or valence band [25,26]. In contrast, the conduction and valence bands of Cr_2COF MXene are mainly from $Cr-d_{x^2-y^2/xy}$ and $Cr-d_{xz/yz}$, respectively, giving rise to sizable valley polarization in both conduction and valence bands. With these results in hand, we can easily understand why the valley polarization in the conduction and valence bands both are sizeable.

To study the valley-dependent physics in Cr_2COF MXene, we calculate the Berry curvature Ω based on the following formula [59]:

$$\Omega_n(\mathbf{k}) = -\sum_{n\neq n'}\frac{2Im\langle\psi_{nk}|v_x|\psi_{n'k}\rangle\langle\psi_{n'k}|v_y|\psi_{nk}\rangle}{(E_n - E_{n'})^2},$$

$$\Omega(\mathbf{k}) = -\sum_n\sum_{n\neq n'}f_n\frac{2Im\langle\psi_{nk}|v_x|\psi_{n'k}\rangle\langle\psi_{n'k}|v_y|\psi_{nk}\rangle}{(E_n - E_{n'})^2}.$$

Here, f_n, $E_n(k)$, and $v_{x/y}$ are the Fermi-Dirac distribution function, eigenvalue of the bloch state ψ_{nk}, and velocity operator, respectively. The valence band is selected to calculate the Berry curvature. The calculated Berry curvature of Cr_2COF MXene as a counter map over the 2D Brillouin zone is shown in Fig. 3(a). Large Ω peaks locate at the $+K$ valleys, while slight Ω peaks appear at the $-K$ valley. Based on this feature, the AVH effect can be observed. Benefited from the large valley polarization in both the valence and conduction bands, the observation of the AVH effect would be rather feasible through electron or hole doping. As illustrated in Fig. 3(b), when shifting the Fermi level between the $+K$ and $-K$ valleys in the conduction band under electron doping, the spin-up electron from the $+K$ valley will gain a vertical velocity and accumulate at the upper edge of the sample under an in-plane electric field, resulting in the AVH effect. On the other hand, through moving the Fermi level between $+K$ and $-K$ valleys in the valence band under hole doping, the spin-down holes from the $+K$ valley will acquire an opposite vertical velocity and gather at the lower edge of the sample under the opposite in-plane electric filed, which generates the AVH effect as well.

Another interesting point we can see from Fig. 3(a) is that the signs of Berry curvature of Cr_2COF MXene at the $+K$ and $-K$ valleys are the same. This is in sharp contrast to the cases of most 2D valleytronic systems wherein the Berry curvature at the $+K$ and $-K$ valleys usually exhibit opposite signs. This phenomenon implies that the valley-dependent band inversion occurs in Cr_2COF MXene. To confirm this point, we plot the orbital-resolved band structure of Cr_2COF MXene without considering SOC in Figs. 2(e) and 2(f). Without considering SOC, the valleys in the conduction and valence bands are dominated by $d_{x^2-y^2/xy}$ orbitals of the Cr_2 atom and $d_{xz/yz}$ orbitals of the Cr_1 atom, respectively. Upon including SOC, as shown in Figs. 2(c) and 2(d), the $+K$ valley in the conduction and valence bands are dominated by $d_{xz/yz}$ orbitals of the Cr_1 atom and $d_{x^2-y^2/xy}$ orbitals of the Cr_2 atom, respectively.
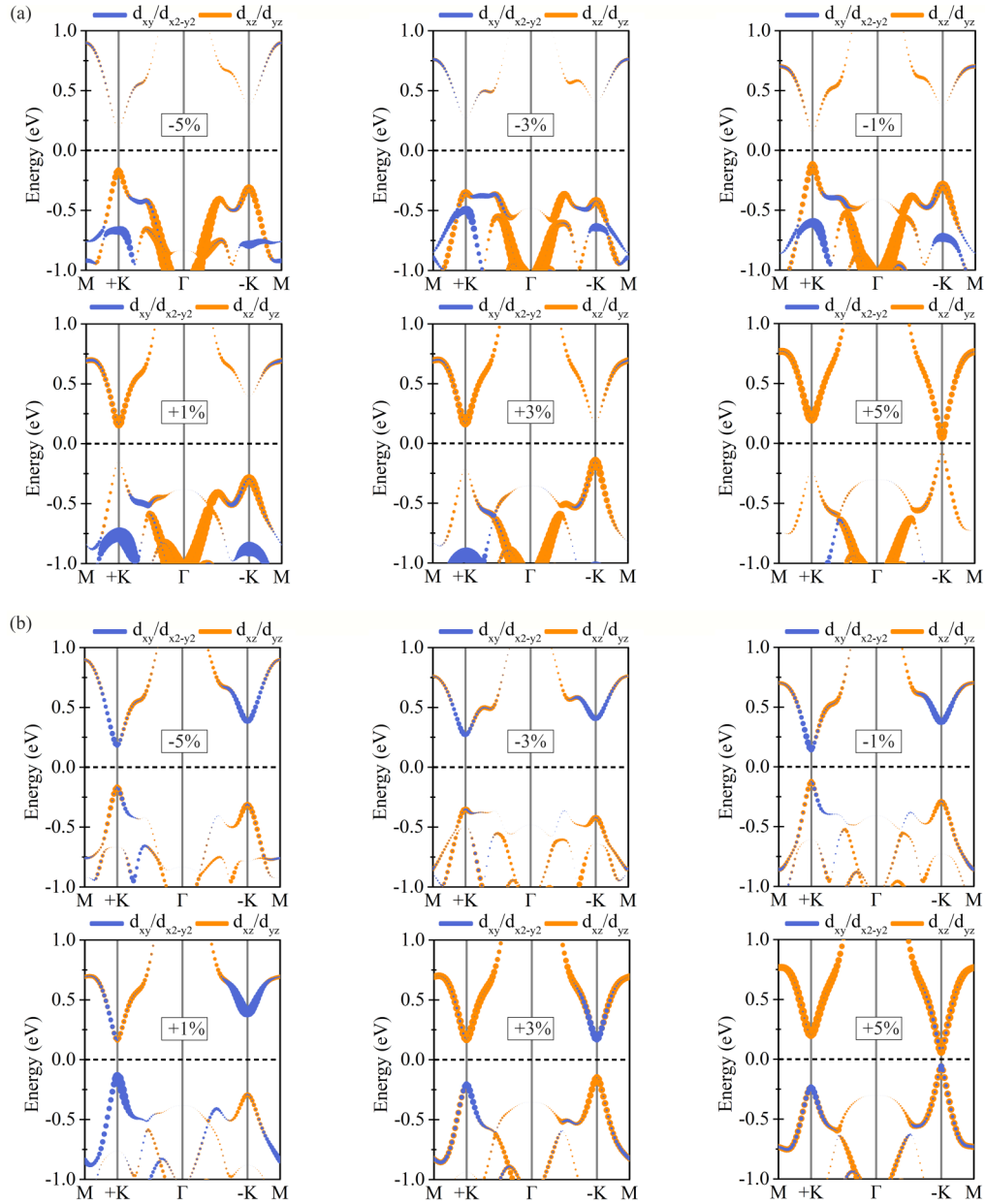
FIG. 4. Orbital-resolved band structures of Cr_2COF MXene with considering spin-orbit coupling (SOC) under various strain projected on the d orbitals of (a) Cr_1 and (b) Cr_2. The Fermi level is set to the valence band maximum.

Therefore, the band order is inverted at the $+K$ valley, while that at the $-K$ valley remains trivial. It should be noted that the band inversion here is not accompanied with the M- or W-shaped band edges, which is like the case of H-FeCl$_2$ [30]. This valley-dependent band inversion clearly indicates the VP-QAH effect in Cr_2COF MXene. To establish this non-trivial topological state of Cr_2COF MXene, we calculate the topological invariants C using the following expression [60]:

$$C = \frac{1}{2\pi} \sum_n \int d^2k \, \Omega_n.$$

With integrating Berry curvature for the whole first Brillouin zone around each individual valley, the Chern number of Cr_2COF MXene is calculated to be C = 1, confirming the

VP-QAH effect. Remarkably, the appearance of the VP-QAH effect does not deform the AVH effect. Generally, the appearance of the VP-QAH effect will deform the band edges and thus valley features, accompanied with the vanishing of the AVH effect. However, in Cr_2COF, the appearance of the VP-QAH effect does not deform the AVH effect. Therefore, Cr_2COF MXene simultaneously exhibits AVH and VP-QAH effects, thus presenting the intriguing valley-related multiple Hall effects.

We further examine the robustness of the valley-related multiple Hall effects in Cr_2COF MXene in terms of strain engineering. Here, biaxial strain is considered, which is defined as $\varepsilon = (a - a_0)/a_0$ (a and a_0 represent the lattice constants of Cr_2COF MXene with and without strain, respectively). The band structures of Cr_2COF MXene with considering SOC
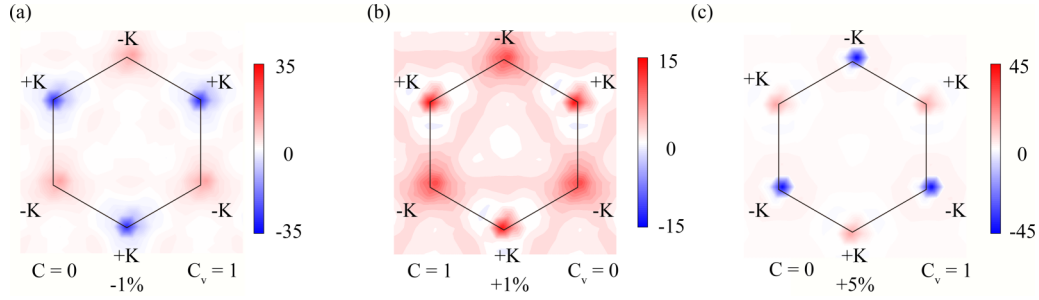
FIG. 5. Berry curvature of Cr_2COF MXene under various strain as a counter map over the two-dimensional (2D) Brillouin zone, where C and C_v represent total and valley-resolved Chern numbers, respectively.

under various strain are displayed in Fig. 4. Here, we assume that the magnetization orientation is along the out-of-plane direction, which will be discussed later. When introducing compressive strain, a band inversion occurs at the $+K$ valleys, resulting in a trivial band order at the $+K$ point. While the band order is preserved at the $-K$ valley, this band inversion leads to a nontrivial-to-trivial phase transition. In this regard, the VP-QAH effect disappears, and the valley-related multiple Hall effects in Cr_2COF MXene degenerate into the AVH effect. The critical transition point is between the strain of -1 and 0%. When applying the tensile strain of 1 and 3%, the band orders at the $+K$ and $-K$ points are like that of the pristine case, indicating the valley-related multiple Hall effects are preserved. Upon increasing the tensile strain to 5%, another band inversion occurs at the $-K$ valley, which gives rise to a nontrivial-to-trivial transition in Cr_2COF MXene. As a result, the VP-QAH effect disappears, and the valley-related multiple Hall effects degenerate into the AVH effect as well. The corresponding critical point for this transition is between the strain of 3 and 5%.

To further confirm the intriguing transitions engineered by strain, taking the cases under strain of -1, 1, and $+5$% as examples, we calculate their Berry curvatures. As shown in Fig. 5, under the strain of 1%, the signs of Berry curvature at $+K$ and $-K$ valleys are identical to the case without strain. For Cr_2COF Mxene under -1% strain, the sign of the Berry curvature at the $+K$ valley becomes negative, indicating a band inversion occurs at the $+K$ valley as compared with the pristine case, while for the case under 5% strain, the sign of the Berry curvature at the $-K$ valley becomes negative, which suggests a band inversion at the $-K$ valley as compared with

the pristine case. This appearance of opposite signs of the of Berry curvature at $+K$ and $-K$ valleys is accompanied with the disappearance of the nontrivial states [28], which agrees well with the above analysis. This topological phase transition is also confirmed by calculating the total and valley resolved Chern numbers.

At last, we investigate the strain effect on MAE and magnetic exchange interaction of Cr_2COF Mxene. As shown in Fig. 6, the FM ground state of Cr_2COF MXene is preserved under the strain of -5 to 5%. For Cr_2COF MXene under strain of -3 to -5% and 5%, the magnetization orientation is shifted to in plane. In this case, the valley polarization disappears (see Fig. S2 in the Supplemental Material [50]), thus vanishing the AVH effect, while for the cases under the strain of 1 and 3%, the out-of-plane magnetization orientation is preserved, ensuring the valley-related multiple Hall effects. Therefore, under strain of 1 and 3%, the valley-related multiple Hall effects are maintained. Under strain of -1%, Cr_2COF MXene only exhibit the AVH effect. For Cr_2COF MXene under strain of -3, -5, and 5%, neither AVH effect nor VP-QAH effect can be observed. As a result, strain can be used to modulate the Hall effects in Cr_2COF MXene.

IV. CONCLUSIONS

To summarize, using first-principles calculations, we study the valley-dependent properties of Cr_2COF MXene. We find that Cr_2COF MXene is a FM semiconductor with valley physics. Due to the intrinsic time-reversal symmetry breaking and out-of-plane magnetization, the valleys are polarized spontaneously. In contrast to 2D valleytronic systems reported
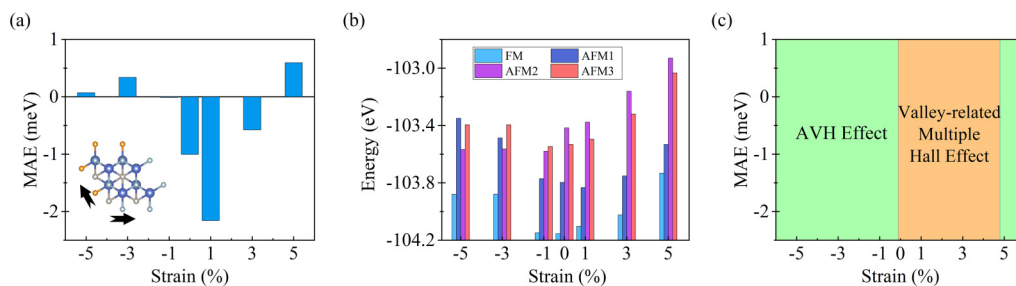

FIG. 6. (a) Magnetic anisotropy energy (MAE) and (b) energies of different magnetic configurations of Cr_2COF MXene as a function of strain. (c) The phase diagram as the function of strain.

in previous works, the valley polarization is sizeable in both the valence and conduction bands, which relates to the particular orbital contribution of the band edges. This sizeable valley polarization is in favor of realizing the AVH effect in Cr_2COF MXene. Moreover, the nontrivial band inversion at the $+K$ valley can be induced by SOC, resulting in the VP-QAH effect. The simultaneously existence of AVH and VP-QAH effects yields the long-sought intrinsic valley-related multiple Hall effects in Cr_2COF MXene. The underlying physics are discussed in detail. In addition, we further reveal that the valley-related multiple Hall effects can be effectively engineered by strain.

[1] D. Xiao, W. Yao, and Q. Nau, Valley-Contrasting Physics in Graphene: Magnetic Moment and Topological Transport, Phys. Rev. Lett. **99**, 236809 (2007).

[2] X. Xu, W. Yao, D. Xiao, and T. F. Heinz, Spin and pseudospins in layered transition metal dichalcogenides, Nature Phys. **10**, 343 (2014).

[3] Z.-M. Yu, S. Guan, X.-L. Sheng, W. Gao, and S. A. Yang, Valley-Layer Coupling: A New Design Principle for Valleytronics, Phys. Rev. Lett. **124**, 037701 (2020).

[4] A. Rycerz, J. Tworzydło, and C. W. J. Beenakker, Valley filter and valley valve in graphene, Nat. Phys. **3**, 172 (2007).

[5] W. Yao, D. Xiao, and Q. Niu, Valley-dependent optoelectronics from inversion symmetry breaking, Phys. Rev. B **77**, 235406 (2008).

[6] D. Xiao, G. Liu, W. Feng, X. Xu, and W. Yao, Coupled Spin and Valley Physics in Monolayers of MoS_2 and Other Group-VI Dichalcogenides, Phys. Rev. Lett. **108**, 196802 (2012).

[7] T. Cao, G. Wang, W. Han, H. Ye, C. Zhu, J. Shi, Q. Niu, P. Tan, E. Wang, B. Liu, and J. Feng, Valley-selective circular dichroism of monolayer molybdenum disulphide, Nat. Commun. **3**, 887 (2012).

[8] J. R. Schaibley, H. Yu, G. Clark, P. Rivera, J. S. Ross, K. L. Seyler, W. Yao, and X. Xu, Valleytronics in 2D materials, Nat. Rev. Mater. **1**, 16055 (2016).

[9] K. F. Mak, K. He, J. Shan, and T. F. Heinz, Control of valley polarization in monolayer MoS_2 by optical helicity, Nat. Nanotech. **7**, 494 (2012).

[10] H. Zeng, J. Dai, W. Yao, D. Xiao, and X. Cui, Valley polarization in MoS_2 monolayers by optical pumping, Nat. Nanotech. **7**, 490 (2012).

[11] P. Rivera, K. L. Seyler, H. Yu, J. R. Schaibley, J. Yan, D. G. Mandrus, W. Yao, and X. Xu, Valley-polarized exciton dynamics in a 2D semiconductor heterostructure, Science **351**, 688 (2016).

[12] L. Li, L. Shao, X. Liu, A. Gao, H. Wang, B. Zheng, G. Hou, K. Shehzad, L. Yu, F. Miao, and Y. Shi, Room-temperature valleytronic transistor, Nat. Nanotech. **15**, 743 (2020).

[13] X. Xu, Y. Ma, T. Zhang, C. Lei, B. Huang, and Y. Dai, Nonmetal-atom-doping-induced valley polarization in single-layer Tl_2O, J. Phys. Chem. Lett. **10**, 4535 (2019).

[14] L. Xu, M. Yang, L. Shen, J. Zhou, T. Zhu, and Y. P. Feng, Large valley splitting in monolayer WS_2 by proximity coupling to an insulating antiferromagnetic substrate, Phys. Rev. B **97**, 041405(R) (2018).

[15] T. Norden, C. Zhao, P. Zhang, R. Sabirianov, A. Petrou, and H. Zeng, Giant valley splitting in monolayer WS_2 by magnetic proximity effect, Nat. Commun. **10**, 4163 (2019).

[16] G. Aivazian, Z. Gong, A. M. Jones, R.-L. Chu, J. Yan, D. G. Mandrus, C. Zhang, D. Cobden, W. Yao, and X. Xu, Magnetic control of valley pseudospin in monolayer WSe_2, Nat. Phys. **11**, 148 (2015).

[17] X. X. Zhang, T. Cao, Z. Lu, Y. C. Lin, F. Zhang, Y. Wang, Z. Li, J. C. Hone, J. A. Robinson, D. Smirnov, S. G. Louie, and T. F. Heinz, Magnetic brightening and control of dark excitons in monolayer WSe_2, Nat. Nanotech. **12**, 883 (2017).

[18] R. Peng, Y. Ma, S. Zhang, B. Huang, and Y. Dai, Valley polarization in Janus single-layer MoSSe via magnetic doping, J. Phys. Chem. Lett. **9**, 3612 (2018).

[19] B. Zhou, Z. Li, J. Wang, X. Niu, and C. Luan, Tunable valley splitting and an anomalous valley Hall effect in hole-doped WS_2 by proximity coupling with a ferromagnetic MnO_2 monolayer, Nanoscale **11**, 13567 (2019).

[20] W. Y. Tong, S. J. Gong, X. Wan, and C.-G. Duan, Concepts of ferrovalley material and anomalous valley Hall effect, Nat. Commun. **7**, 13612 (2016).

[21] J. Liu, W. J. Hou, C. Cheng, H. X. Fu, J. T. Sun, and S. Meng, Intrinsic valley polarization of magnetic VSe_2 monolayers, J. Phys. Condens. Matter **29**, 255501 (2017).

[22] P. Zhao, Y. Ma, C. Lei, H. Wang, B. Huang, and Y. Dai, Single-layer $LaBr_2$: Two-dimensional valleytronic semiconductor with spontaneous spin and valley polarizations, Appl. Phys. Lett. **115**, 261605 (2019).

[23] Q. Cui, Y. Zhu, J. Liang, P. Cui, and H. Yang, Spin-valley coupling in a two-dimensional VSi_2N_4 monolayer, Phys. Rev. B **103**, 085421 (2021).

[24] Y. Zhang, Y. Ma, R. Peng. H. Wang, B. Huang, and Y. Dai, Large valley-polarized state in single-layer NbX_2 ($X = S$, Se): theoretical prediction, Nano Res. **14**, 834 (2021).

[25] Z. He, R. Peng, X. Feng, X. Xu, Y. Dai, B. Huang, and Y. Ma, Two-dimensional valleytronic semiconductor with spontaneous spin and valley polarization in single-layer Cr_2Se_3, Phys. Rev. B **104**, 075105 (2021).

[26] H. X. Cheng, J. Zhou, W. Ji, Y. N. Zhang, and Y. P. Feng, Two-dimensional intrinsic ferrovalley GdI_2 with large valley polarization, Phys. Rev. B **103**, 125121 (2021).

[27] H. Pan, Z. Li, C. Liu, G. Zhu, Z. Qiao, and Y. Yao, Valley-Polarized Quantum Anomalous Hall Effect in Silicene, Phys. Rev. Lett. **112**, 106802 (2014).

[28] J. Zhou, Q. Sun, and P. Jena, Valley-Polarized Quantum Anomalous Hall Effect in Ferrimagnetic Honeycomb Lattices, Phys. Rev. Lett. **119**, 046403 (2017).

[29] T. Zhou, J. Zhang, H. Jiang, Igor Žutić, and Z. Yang, Giant spin-valley polarization and multiple Hall effect in functionalized bismuth monolayers, npj Quant. Mater. **3**, 39 (2018).

[30] H. Hu, W.-Y. Tong, Y.-H. Shen, X. Wan, and C.-G. Duan, Concepts of the half-valley-metal and quantum anomalous valley Hall effect, npj Comput. Mater. **6**, 129 (2020).

[31] C. Chang, J. Zhang, X. Feng, J. Shen, Z. Zhang, M. Guo, K. Li, Y. Ou, P. Wei, L. Wang, Z. Ji, Y. Feng, S. Ji, X. Chen, J. Jia, X. Dai, Z. Fang, S. Zhang, K. He, Y. Wang, L. Lu, X. Ma, and Q. Xue, Experimental observation of the quantum anomalous Hall effect in a magnetic topological insulator, Science **340**, 167 (2013).

[32] Y. Deng, Y. Yu, M. Shi, Z. Guo, Z. Xu, J. Wang, X. Chen, and Y. Zhang, Quantum anomalous Hall effect in intrinsic magnetic topological insulator MnBi$_2$Te$_4$, Science **367**, 6480 (2020).

[33] H. Weng, R. Yu, X. Hu, X. Dai, and Z. Fang, Quantum anomalous Hall effect and related topological electronic states, Adv. Phys. **64**, 227 (2015).

[34] T. Zhou, J. Zhang, B. Zhao, H. Zhang, and Z. Yang, Quantum spin-quantum anomalous Hall insulators and topological transitions in functionalized Sb(111) monolayers, Nano Lett. **15**, 5149 (2015).

[35] T. Zhou, J. Zhang, B. Y. Xue, B. Zhao, H. Zhang, H. Jiang, and Z. Yang, Quantum spin-quantum anomalous Hall effect with tunable edge states in Sb monolayer-based heterostructures, Phys. Rev. B **94**, 235449 (2016).

[36] H. Zhang, W. Yang, Y. Ning, and X. Xu, Abundant valley-polarized states in two-dimensional ferromagnetic van der Waals heterostructures, Phys. Rev. B **101**, 205404 (2020).

[37] H. Huan, Y. Xue, B. Zhao, G. Gao, H. Bao, and Z. Yang, Strain-induced half-valley metals and topological phase transitions in MBr$_2$ monolayers (M = Ru, Os), Phys. Rev. B **104**, 165427 (2021).

[38] M. Naguib, M. Kurtoglu, V. Presser, J. Lu, J. Niu, M. Heon, L. Hultman, Y. Gogotsi, and M. W. Barsoum, Two-dimensional nanocrystals produced by exfoliation of Ti$_3$AlC$_2$, Adv. Mater. **23**, 4248 (2011).

[39] M. Naguib, V. N. Mochalin, M. W. Barsoum, and Y. Gogotsi, 25th anniversary article: MXenes: A new family of two-dimensional materials, Adv. Mater. **26**, 992 (2014).

[40] P. E. Blöchl, Projector augmented-wave method, Phys. Rev. B **50**, 17953 (1994).

[41] G. Kresse and J. Hafner, *Ab initio* molecular-dynamics simulation of the liquid-metal–amorphous-semiconductor transition in germanium, Phys. Rev. B **49**, 14251 (1994).

[42] G. Kresse and J. Furthmüller, Self-interaction correction to density functional approximation for many electron systems, Phys. Rev. B **54**, 11169 (1996).

[43] J. P. Perdew, K. Burke, and M. Ernzerhof, Generalized Gradient Approximation Made Simple, Phys. Rev. Lett. **77**, 3865 (1996).

[44] J. Heyd, G. E. Scuseria, and M. Ernzerhof, Hybrid functionals based on a screened Coulomb potential, J. Chem. Phys. **118**, 8207 (2003).

[45] F. Takahiro, H. Yasuhiro, and S. Hiroshi, Chern numbers in discretized Brillouin zone: Efficient method of computing (spin) Hall conductances, J. Phys. Soc. Jpn. **74**, 1674 (2005).

[46] S. Li, J. He, L. Grajciar, and P. Nachtigall, Intrinsic valley polarization in 2D magnetic MXenes: Surface engineering induced spin-valley coupling, J. Mater. Chem. C **9**, 11132 (2021).

[47] B. Goodenough, Theory of the role of covalence in the Perovskite-type manganites [La, M(II)] MnO$_3$, Phys. Rev. **100**, 564 (1955).

[48] J. Kanamori, Superexchange interaction and symmetry properties of electron orbitals, J. Phys. Chem. Solids **10**, 87 (1959).

[49] P. W. Anderson, New approach to the theory of superexchange interactions, Phys. Rev. **115**, 2 (1959).

[50] See Supplemental Material at http://link.aps.org/supplemental/10.1103/PhysRevMaterials.6.044001 for more details on the magnetic configurations and electronic properties of Cr$_2$COF MXene.

[51] S. V. Halilov, A. Ya. Perlov, P. M. Oppeneer, A. N. Yaresko, and V. N. Antonov, Magnetocrystalline anisotropy energy in cubic Fe, Co, and Ni: Applicability of local-spin-density theory reexamined, Phys. Rev. B **57**, 9557 (1998).

[52] W. Zhang, Q. Qu, P. Zhu, and C. Lam, Robust intrinsic ferromagnetism and half semiconductivity in stable two-dimensional single-layer chromium trihalides, J. Mater. Chem. C **3**, 12457 (2015).

[53] B. Huang, G. Clark, E. Navarro-Moratalla, D. R. Klein, R. Cheng, K. L. Seyler, D. Zhong, E. Schmidgall, M. A. McGuire, D. H. Cobden, W. Yao, D. Xiao, P. Jarillo-Herrero, and X. Xu, Layer-dependent ferromagnetism in a van der Waals crystal down to the monolayer limit, Nature (London) **546**, 270 (2017).

[54] Z. Gao, F. Ma, X. Zhang, Z. Tian, Y. Liu, Y. Jiao, and A. Du, Predicting MnB$_6$ monolayer with room temperature ferromagnetism and high magnetic anisotropy, Physica. E **134**, 114930 (2021).

[55] H. Zeng, Y. Bao, Z. Chen, Y. Hu, J. Wang, and X. Fan, High-temperature ferromagnetism in monolayers MnGaX_3 (X = Te, Se), J. Magn. Magn. Mater. **534**, 168041 (2021).

[56] N. D. Mermin and H. Wanger, Absence of Ferromagnetism or Antiferromagnetism in One- or Two-Dimensional Isotropic Heisenberg Models, Phys. Rev. Lett. **17**, 1133 (1966).

[57] M.-H. Whangbo, E. E. Gordon, H. Xiang, H.-J. Koo, and C. Lee, Prediction of spin orientations in terms of HOMO-LUMO interactions using spin-orbit coupling as perturbation, Acc. Chem. Res. **48**, 3080 (2015).

[58] M.-H. Whangbo, H. Xiang, H.-J. Koo, E. E. Gordon, and J. L. Whitten, Electronic and structural factors controlling the spin orientations of magnetic ions, Inorg. Chem. **58**, 11854 (2019).

[59] D. J. Thouless, M. Kohmoto, M. P. Nightingale, and M. den Nijs, Quantized Hall Conductance in a Two-Dimensional Periodic Potential, Phys. Rev. Lett. **49**, 405 (1982).

[60] Y. G. Yao, L. Kleinman, A. H. MacDonald, J. Sinova, T. Jungwirth, D.-S. Wang, E. Wang, and Q. Niu, First Principles Calculation of Anomalous Hall Conductivity in Ferromagnetic bcc Fe, Phys. Rev. Lett. **92**, 037204 (2004).